BIOCHEMISTRY
including biophysical chemistry & molecular biology

Article

pubs.acs.org/biochemistry

Imprint of Ancient Evolution on rRNA Folding

Kathryn A. Lanier,[†] Shreyas S. Athavale,[†] Anton S. Petrov,[†] Roger Wartell,[‡] and Loren Dean Williams*[,†]

[†]School of Chemistry and Biochemistry and [‡]School of Biology, Georgia Institute of Technology, Atlanta, Georgia 30332-0400, United States

Supporting Information

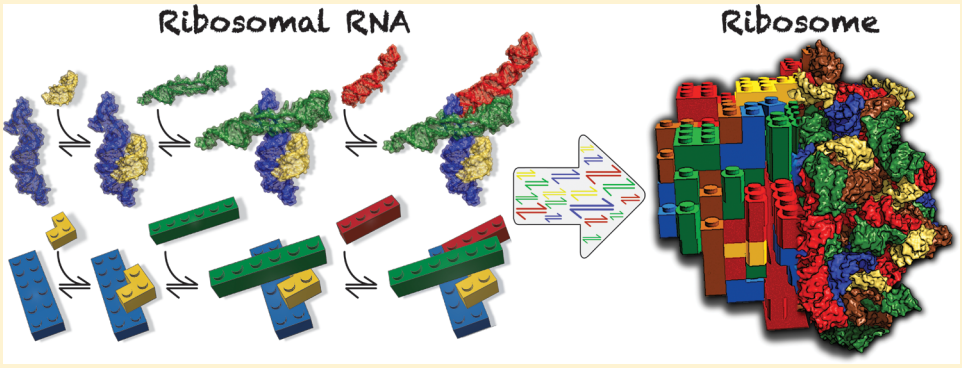

ABSTRACT: In a model describing the origin and evolution of the translation system, ribosomal RNA (rRNA) grew in size by accretion [Petrov, A. S., et al. (2015) History of the Ribosome and the Origin of Translation. *Proc. Natl. Acad. Sci. U.S.A. 112*, 15396−15401]. Large rRNAs were built up by iterative incorporation and encasement of small folded RNAs, in analogy with addition of new LEGOs onto the surface of a preexisting LEGO assembly. In this model, rRNA robustness in folding arises from inherited autonomy of local folding. We propose that rRNAs can be decomposed at various granularities, retaining folding mechanism and folding competence. To test these predictions, we disassembled Domain III of the large ribosomal subunit (LSU). We determined whether local rRNA structure, stability, and folding pathways are autonomous. Thermal melting, chemical footprinting, and circular dichroism were used to infer rules that govern folding of rRNA. We deconstructed Domain III of the LSU rRNA by mapping out its complex multistep melting pathway. We studied Domain III and two equal-size "sub-Domains" of Domain III. The combined results are consistent with a model in which melting transitions of Domain III are conserved upon cleavage into sub-Domains. Each of the eight melting transitions of Domain III corresponds in T_m and ΔH with a transition observed in one of the two isolated sub-Domains. The results support a model in which structure, stability, and folding mechanisms are dominated by local interactions and are unaffected by separation of the sub-Domains. Domain III rRNA is distinct from RNAs that form long-range cooperative interaction networks at early stages of folding or that do not fold reversibly.

We recently proposed the accretion model, which is a molecular level description of the origins and evolution of the ribosome.[1,2] This model, based on a three-dimensional comparative method, makes predictions about mechanisms and robustness of ribosomal RNA (rRNA) folding. In the accretion model, small folding competent RNAs were subsumed onto subunit surfaces, gradually encasing and freezing previously acquired rRNA. The acquisition of new rRNA did not perturb previously deposited rRNA. In this model, rRNA growth is analogous to the addition of new LEGOs onto the surface of a preexisting LEGO assembly.[3]

The accretion model makes predictions about the properties of rRNAs. One prediction is that rRNAs, even though they are immense in size, are robust in folding. The model suggests that rRNA robustness in folding arises from inherited autonomy of local folding. Local autonomy should be retained at all stages of folding, even during complex sequential progressions characteristic of folding of large RNAs. Local contributions of rRNAs are predicted to add in a conservative fashion at all stages of folding. rRNA should be decomposable into elements that retain folding mechanisms in isolation of each other. The experiments here are designed to test these predictions.

Here we cleave an rRNA domain from the large ribosomal subunit (LSU) and further section it into two sub-Domains. To test predictions of the accretion model, we characterize the structure, local and global stability, and folding pathways of the rRNA elements. We ask if local rRNA elements are continuously autonomous throughout their folding pathways and if their contributions during folding add in a conservative fashion. We determine how local components of a large rRNA domain combine to achieve global stability and the extent to which they cooperate during folding. Computation and experiment were used to infer rules that govern folding at various scales. Folding pathways and conformation were characterized by thermal melting experiments, chemical footprinting, and circular dichroism (CD) spectroscopy.

Received: February 22, 2016
Revised: July 12, 2016
Published: July 18, 2016

ACS Publications © 2016 American Chemical Society

DOI: 10.1021/acs.biochem.6b00168
Biochemistry 2016, 55, 4603−4613

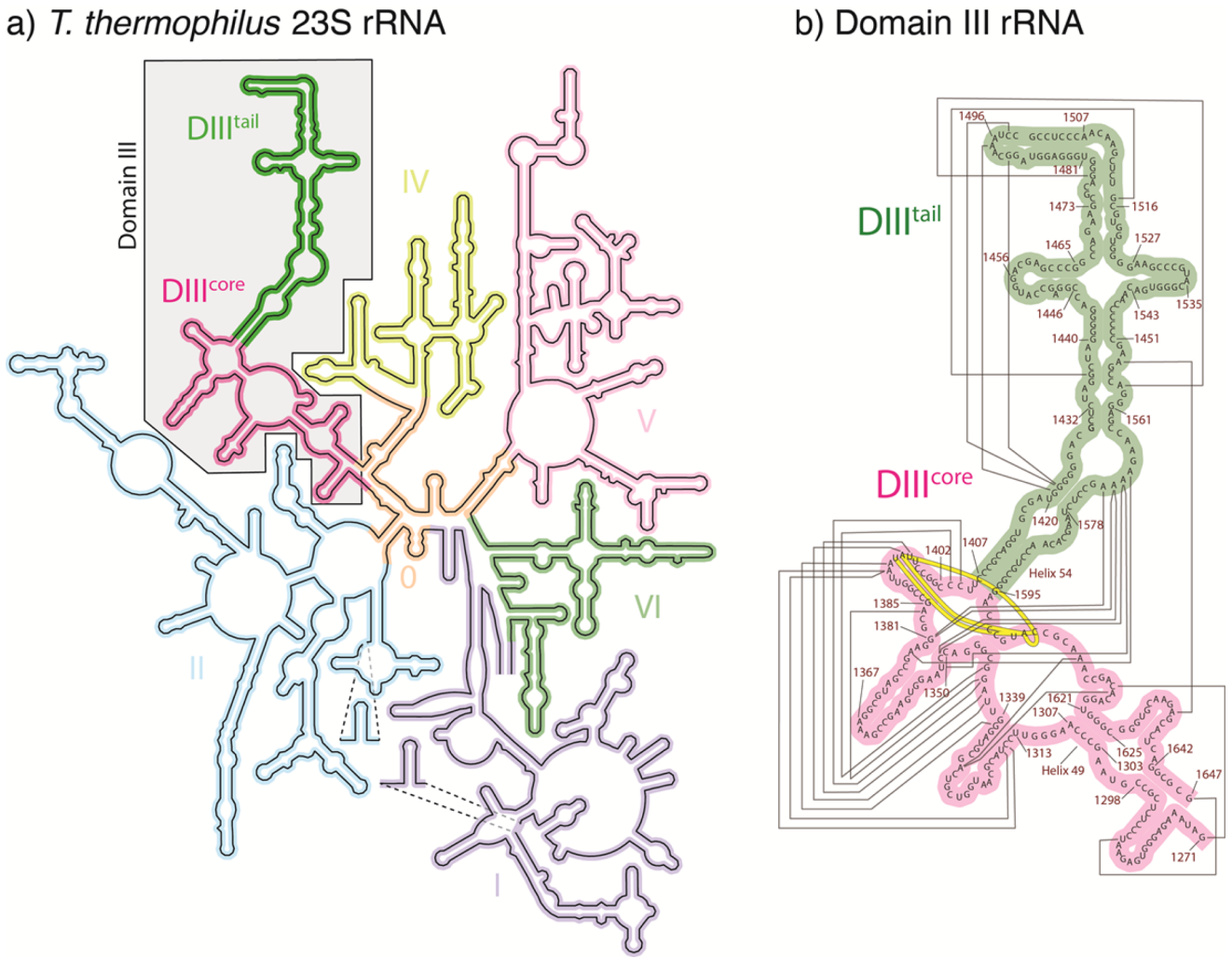

Figure 1. (a) Secondary structure of the 23S rRNA of *Thermus thermophilus* (PDB entry 1VY4).[11] Domains are distinguished by color. Domain III is shaded. DIII^{core} is colored magenta and DIII^{tail} green. (b) Secondary structure of Domain III rRNA, indicating DIII^{core} and DIII^{tail}. The yellow lines are first-shell phosphate−Mg^{2+}−phosphate interactions within the Mg^{2+} microcluster. Gray lines are base−base tertiary interactions as determined by FR3D.[12] Nucleotides are numbered according to the *Escherichia coli* numbering system.

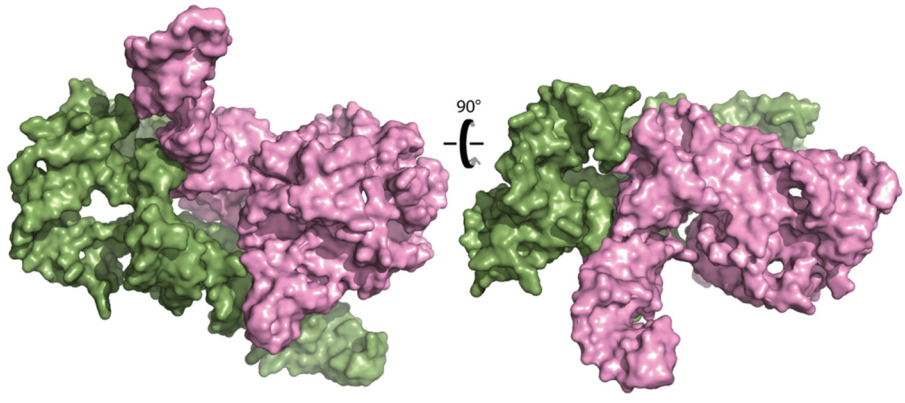

Figure 2. Surface representation of Domain III in three dimensions as observed in the intact ribosome. DIII^{core} is colored magenta and DIII^{tail} green, as in Figure 1 (PDB entry 1VY4).

We deconstructed Domain III of the LSU rRNA by mapping out its multistep melting pathway. We cleaved Domain III from the rest of the 23S rRNA at an insertion fingerprint.[1,2] An insertion fingerprint marks the site of an rRNA expansion. Comparison of pre- and postexpanded rRNAs in three dimensions reveals the points at which ancestral rRNA is joined to more recent rRNA. New rRNA is added to old rRNA with preservation of the local conformation and of structural integrity of the old rRNA. We characterized Domain III and two equal-size sub-Domains of Domain III. The two independent sub-Domains,

DOI: 10.1021/acs.biochem.6b00168
Biochemistry 2016, 55, 4603−4613

sub-Domain III^{core} (DIII^{core}) and sub-Domain III^{tail} (DIII^{tail}), were created by splitting Domain III, as shown in Figures 1 and 2. Domain III was cleaved within Helix 54, which was then capped with a stem−loop (Figure S1) to maintain the unimolecular character of DIII^{core} and to preserve its secondary structure.[4] We determined that local folding mechanisms are independent of context as predicted by the accretion model. This work has analogy with previous efforts with proteins[5−7] and folded mRNAs.[8−10] The combined data presented here are consistent with the accretion model of ribosomal evolution.

MATERIALS AND METHODS

rRNA Sequences. Nucleotide sequences of Domain III, DIII^{core}, and DIII^{tail} were obtained from the 23S rRNA of *Thermus thermophilus*. For the construction of DIII^{core}, two rRNA fragments were joined together, with a GNRA tetraloop, to form a single strand of rRNA (Figure S1). Cleaving the domain and resealing the fragments within a helical region facilitate formation of the nativelike secondary structure of DIII^{core} but do not influence the three-dimensional structure.[4] rRNAs were synthesized and purified as described in the Supporting Information. Coordinates of Domain III rRNA were extracted from the crystal structure of the *T. thermophilus* 70S ribosome (PDB entry 1VY4).[13] rRNA−rRNA interactions were identified with FR3D[12] and by inspection of the three-dimensional structure. rRNA−Mg^{2+} interaction geometries were computed directly from the coordinates. First-shell Mg^{2+}−ligand interactions were defined by distances <2.2 Å.[14,15]

SHAPE. Selective 2′-hydroxyl acylation analyzed by primer extension (SHAPE) was performed as described previously.[16] *In vitro*-transcribed rRNA was heated in the presence of chelating resin to remove Mg^{2+} ions. rRNA was folded in the presence or absence of 10 mM $MgCl_2$. rRNA was modified with 13 mM *N*-methylisatoic anhydride (NMIA) (Tokyo Chemical Industry Co., Ltd.) and purified using an RNeasy Mini Kit (Qiagen). A 20-nucleotide DNA oligomer, 5′-CGCGCCTG-AGTGCTCTTGCA-3′, labeled with 6-FAM using a 5′-amino C6 linker (Operon MWG), which anneals to the 3′-end of Domain III and DIII^{core}, was used to prime reverse transcription. Reverse transcription reaction mixtures were resolved on a 3130 Genetic Analyzer (Applied Biosystems). SHAPE data reduction and processing were performed as described in our Supporting Information and in the Supporting Information of ref 16.

Circular Dichroism Spectroscopy. CD spectra were recorded using 1 μM rRNA strand in 180 mM NaCl and 20 mM Tris-HEPES (pH 8.0) in the absence or presence of 0.5 mM $MgCl_2$ (Figure S2) on a Jasco J-810 spectropolarimeter. Four CD spectra were averaged from 350 to 220 nm with an integration time of 4 s, a bandwidth of 4 nm, and a scan speed of 50 nm/min. The temperature was maintained at 20 °C. rRNA concentrations were determined by absorbance at 260 nm.

UV Melting. Absorbance spectra were recorded in 180 mM NaCl and 20 mM Tris-HEPES (pH 8.0) in the absence or presence of 0.5 mM $MgCl_2$. The temperature dependence of UV absorbance was determined for Domain III, DIII^{core}, and DIII^{tail}. Melting curves were obtained by monitoring the UV absorbance at 260 and 280 nm as a function of temperature using a Varian Cary-100 UV spectrophotometer in 1 cm path length quartz cuvettes. Prior to data collection, rRNAs were annealed by being heated to 95 °C and slowly cooled to 15 °C. Forward and reverse melting curves were obtained by heating or cooling at a rate of 1 °C/min. Absorbance values were recorded every 0.2 °C between 25 and 95 °C.

Thermodynamic parameters were obtained from melting curves by nonlinear fitting to a multistate model. Absorbance versus temperature was expressed as fraction of unfolded rRNA, $\theta_u(T)$, as in eq 1.

$$\theta_u(T) = \frac{A(T) - A_{ini}(T)}{A_{fin}(T) - A_{ini}(T)} \quad (1)$$

where $A(T)$ is the absorbance at temperature T and $A_{ini}(T)$ and $A_{fin}(T)$ are the initial and final linear baselines, respectively. Derivatives of $\theta_u(T)$ were taken with respect to temperature using IGOR Pro. Observed $d\theta_u(T)/dT$ versus T plots were fit to multiple melting transitions and analyzed for transition parameters with eq 2, using IGOR Pro.

$$\frac{d\theta_u(T)}{dT} = \sum_n \frac{A_n \frac{\Delta H_n}{2RT^2}}{1 + (T - T_{m,n}) \cosh\left(\frac{\Delta H_n}{RT \times T_{m,n}}\right)} \quad (2)$$

For each unfolding transition, n, A_n is the relative hyperchromicity, ΔH_n is the enthalpy per mole, and $T_{m,n}$ is the melting temperature. The entropy change of each transition was determined by eq 3.

$$\Delta S_n = -\frac{\Delta H_n}{T_{m,n}} \quad (3)$$

where ΔG_n was calculated at 25 °C using ΔH_n and ΔS_n.

Melting profile data were fit to models with increasing numbers of transitions (i.e., one, two, three, four, etc.) to determine the minimal number of transitions needed to predict the observed melting profile, minimizing the standard error. We sought the simplest model for which discrepancies between predicted and observed data were minimal and were random rather than systematic (Figures S3 and S4). More complex models with a greater number of transitions are possible and cannot be excluded by the methods employed here.

The melting profiles of the component rRNAs (DIII^{core} and DIII^{tail}) were added to obtain the calculated melting profile of intact Domain III (Figure S5), which was also obtained experimentally. The equations, in Igor syntax, are provided in the Supporting Information.

RESULTS

Domains and sub-Domains. We determined whether rRNA folding mechanisms are dominated by local interactions or are significantly affected by long-range interactions. Structure, conformation, and unfolding pathways were characterized by thermal melting, chemical footprinting, and CD spectroscopy. Computation and experiment were used to infer rules that govern folding of rRNA at various scales. We isolated Domain III from the large ribosomal subunit and separated it into two sub-Domains, DIII^{core} and DIII^{tail}. We determined whether structure, stability, and unfolding mechanisms of DIII^{core} and DIII^{tail} are conserved when they are excised from Domain III.

SHAPE. Selective 2′-hydroxyl acylation analyzed by primer extension (SHAPE)[17] provides information about secondary structure and, in the presence of magnesium, three-dimensional structure.[16] SHAPE exploits the reactivity of the 2′-hydroxyl groups of RNA with electrophilic reagents such as NMIA. The reactivities of RNA 2′-hydroxyl groups are dependent on local RNA flexibility.[18,19] Paired nucleotides

DOI: 10.1021/acs.biochem.6b00168
Biochemistry 2016, 55, 4603−4613

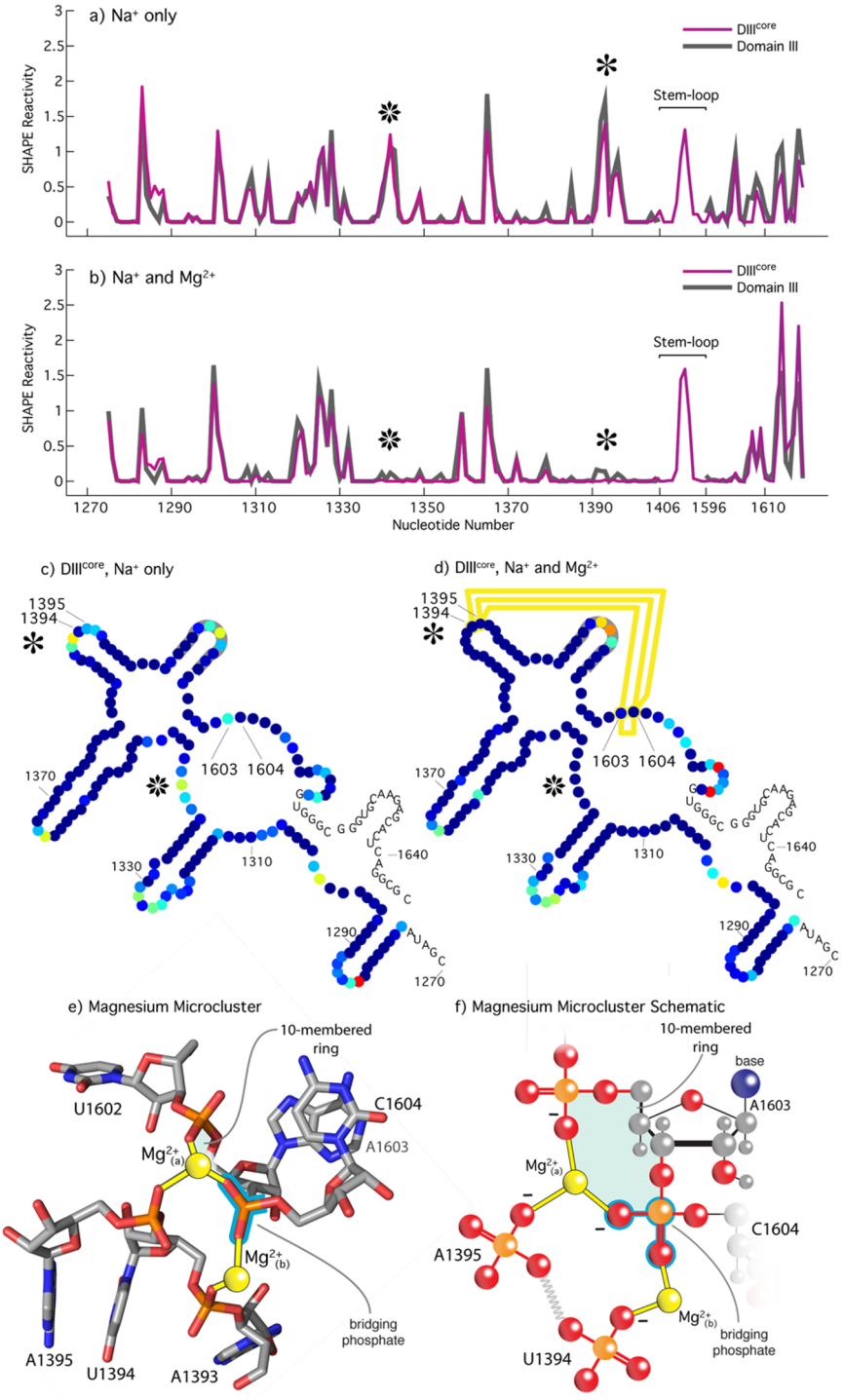

Figure 3. SHAPE reactivities, structures, and Mg^{2+} interactions. (a) SHAPE reactivities of $DIII^{core}$ (magenta) and Domain III (gray) in the presence of 250 mM Na^+ only. (b) SHAPE reactivities of $DIII^{core}$ and Domain III in the presence of 250 mM Na^+ and 10 mM Mg^{2+}. $DIII^{core}$ shows the same reactivity as Domain III under both sets of conditions. The asterisks highlight the regions of the rRNA where the addition of Mg^{2+} causes significant changes in SHAPE reactivity. SHAPE reactivities for $DIII^{core}$ (c) in 250 mM Na^+ only and (d) in 250 mM Na^+ and 10 mM Mg^{2+} mapped onto the secondary structure of $DIII^{core}$. SHAPE reactivity is indicated on a color scale of blue to red, with blue being the least reactive and red being the most reactive. Some Mg^{2+}-dependent nucleotides are observed within a Mg^{2+} microcluster. Mg^{2+}-mediated interactions between rRNA phosphate groups are indicated by yellow lines. The stem−loop sequence used to connect the two fragments is colored gray. (e) Domain III Mg^{2+} microcluster observed in the structure of the native LSU, containing two Mg^{2+} ions linked by a bridging phosphate (colored blue). (f) Schematic diagram of the Mg^{2+} microcluster, highlighting canonical elements of Mg^{2+} microclusters, including the bridging phosphate and the 10-membered ring. The gray zigzag line is a reduced representation of the U1394 nucleoside linkage between the phosphate groups.

are less flexible and are therefore less reactive than unpaired nucleotides. Local RNA flexibility, and therefore SHAPE reactivity, can be altered by tertiary interactions facilitated by Mg^{2+} ions and by direct interaction with Mg^{2+} ions. We have previously described the SHAPE reactions of Domain III in the presence and absence of Mg^{2+}.[16]

DOI: 10.1021/acs.biochem.6b00168
Biochemistry 2016, 55, 4603−4613

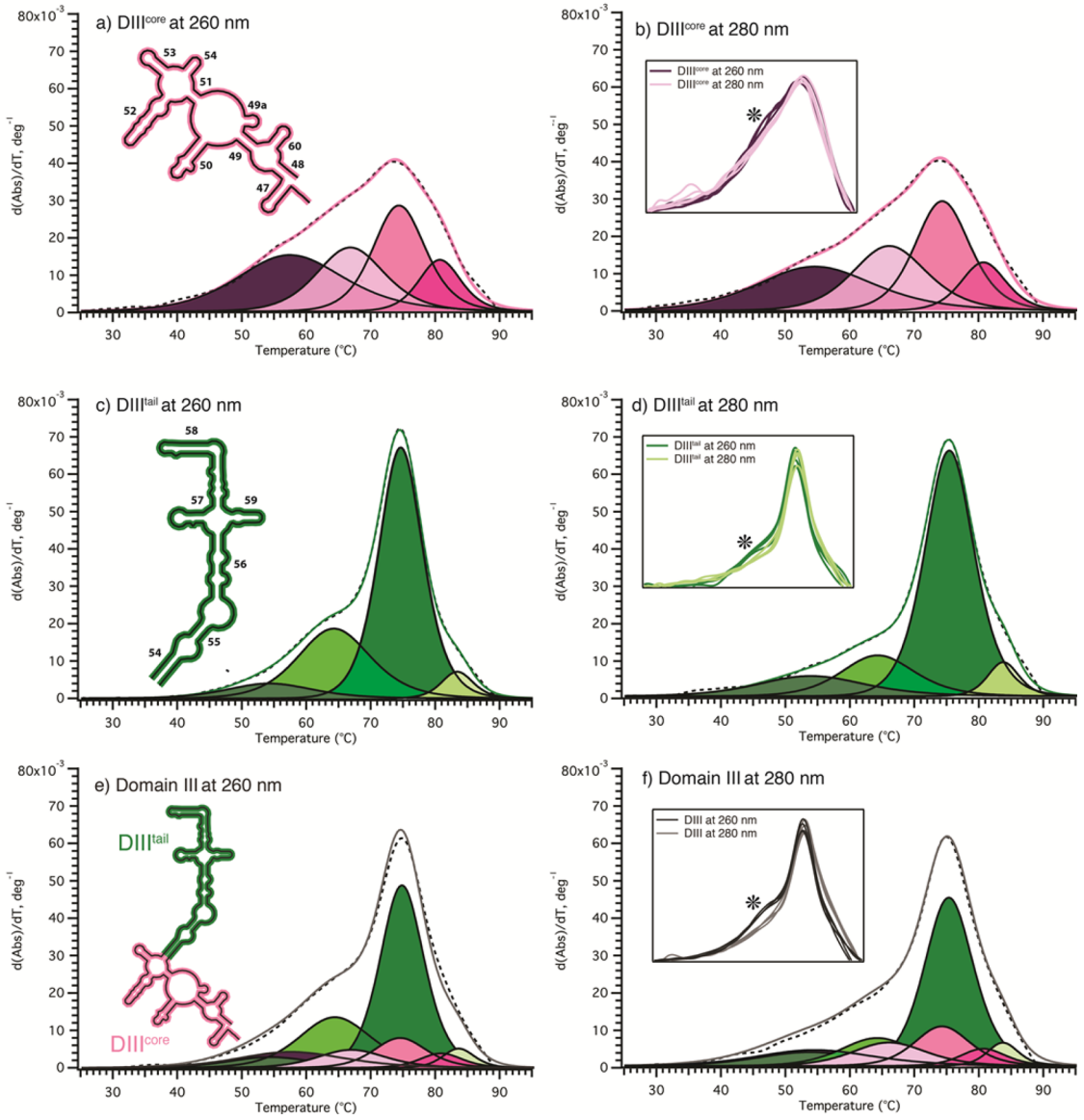

Figure 4. Unfolding mechanism is conserved when Domain III is cleaved into DIII^{core} and DIII^{tail}. Derivative melting profiles are shown for DIII^{core}, DIII^{tail}, and Domain III at 260 and 280 nm. Experimental melting profiles are dashed lines. The fits to the melting profiles are colored solid lines, and the component transitions are black lines with colored fill. (a) DIII^{core} melting profile, fit, and deconvolution at 260 nm. (b) DIII^{core} melting profile at 280 nm. (c) DIII^{tail} melting profile, fit, and deconvolution at 260 nm. (d) DIII^{tail} melting profile at 280 nm. (e) Intact Domain III melting profile and the sum of the component transitions of DIII^{core} and DIII^{tail} at 260 nm. The solid line is a weighted sum of the melting profiles of DIII^{core} and DIII^{tail}. The eight component transitions, obtained from the deconvolution of DIII^{core} and DIII^{tail}, add to give the melting profile of Domain III. (f) Same as panel e at 280 nm. All melting experiments described here were performed in 180 mM NaCl, 20 mM Tris-HEPES, pH 8.0 buffer. Asterisks in the insets indicate the reproducibility of differences in the low-temperature melting behavior when the wavelength is changed from 260 to 280 nm.

DIII^{core} in Na$^+$. The secondary structure of DIII^{core} is conserved when it is excised from Domain III. We used SHAPE to probe the secondary structure of intact Domain III[16] and DIII^{core} in the absence and presence of Mg^{2+} (Figure 3). We hypothesized that in the presence of Na^+ alone, DIII^{core} would assume the same secondary structure that was observed for this segment of the rRNA in the canonical secondary structure of the 23S rRNA[11] and may also form a subset of tertiary interactions[20] as seen in the assembled ribosome.[21,22] SHAPE data obtained here for DIII^{core} in the absence of Mg^{2+} correspond very closely with expectations from canonical 23S rRNA secondary structure. Helical regions show low reactivity, while loops and bulges show high reactivity.

In addition, the SHAPE data indicate that DIII^{core} and the corresponding region of intact Domain III fold to the same state. As illustrated by the overlaid SHAPE traces (Figure 3a), the reactivities of intact Domain III and DIII^{core} are essentially identical along the common regions of the sequence. The high degree of similarity in SHAPE reactivities suggests that the secondary structures of Domain III and isolated DIII^{core} are essentially the same as those of intact 23S rRNA.

DIII^{core} in Na$^+$ and Mg^{2+}. DIII^{core} shows nativelike interactions with Mg^{2+}. In the native state of DIII^{core}, as observed in the three-dimensional structure of the assembled ribosome,[21,22] Mg^{2+} ions mediate backbone−backbone interactions within a Mg^{2+} microcluster (Figure 3e).[15] Previously, we used the Mg^{2+} dependence of SHAPE to show that isolated Domain III folds to a near-native state in the presence of both Na^+ and Mg^{2+}.[16] The effects of Mg^{2+} are localized to specific regions of the rRNA and

DOI: 10.1021/acs.biochem.6b00168
Biochemistry 2016, 55, 4603−4613

are not widely dispersed, suggesting that Mg^{2+} binding sites are preorganized in the presence of Na^{+}. The effects of Mg^{2+} on the SHAPE profiles of $DIII^{core}$ and Domain III[16] are very similar. Mg^{2+}-specific changes in SHAPE of $DIII^{core}$ rRNA are focused primarily on the region of the Mg^{2+} microcluster. The Mg^{2+} dependence of the SHAPE reactivity appears to reflect the effects of specific binding of Mg^{2+} to rRNA on the Mg^{2+} microcluster and on associated tertiary interactions. Before the addition of Mg^{2+}, many of the nucleotides in and around the Mg^{2+} microcluster site have high SHAPE reactivities. After the addition of Mg^{2+}, nucleotides in and around the Mg^{2+} microcluster have significantly lower SHAPE reactivities. The loop centered around U1394 shows a general decrease in SHAPE reactivity upon the addition of Mg^{2+}. A1603 also shows a decrease in SHAPE reactivity.

The observed Mg^{2+} dependence of SHAPE reactivities of Domain III and $DIII^{core}$ is consistent with formation of the Mg^{2+} microcluster (Figure 3e,f) in both rRNAs upon addition of Mg^{2+}. In the three-dimensional structure of the assembled ribosome, this Mg^{2+} microcluster is fully contained within the rRNA corresponding to $DIII^{core}$.[23]

A canonical Mg^{2+} microcluster, as defined by Hsiao et al.,[23] contains two closely associated Mg^{2+} ions that are highly coordinated by phosphate oxygen atoms of the rRNA. Defining features of a Mg^{2+} microcluster are (i) a 10-membered $Mg^{2+}_{(a)}$-(OP-P-O5′-C5′-C4′-C3′-O3′-P-OP)-$Mg^{2+}_{(a)}$ ring and (ii) a phosphate group that bridges two Mg^{2+} ions [$Mg^{2+}_{(a)}$-O1P-P-O2P-$Mg^{2+}_{(b)}$]. Here, the phosphate group of C1604 forms a bridge between two Mg^{2+} ions [$Mg^{2+}_{(a)}$ and $Mg^{2+}_{(b)}$ in Figure 3e,f]. The phosphate group and ribose of A1603 along with the phosphate group of C1604 clamp onto $Mg^{2+}_{(a)}$, combining to form a 10-membered ring. The two Mg^{2+} ions of this Mg^{2+} microcluster are coordinated by the phosphate groups of U1394 and A1395, which are remote in the secondary structure.

Circular Dichroism Spectroscopy. The CD spectra of $DIII^{core}$ and $DIII^{tail}$ add to give the spectrum of Domain III, indicating that the helical content of the sub-Domains is conserved when they are joined to form the complete domain. CD provides empirical fingerprints of secondary structures of chiral polymers. CD data here indicate that secondary structures are conserved between intact Domain III and isolated $DIII^{core}$ and $DIII^{tail}$. The CD spectra of equilimolar $DIII^{core}$ and $DIII^{tail}$ can be added to give the CD spectrum of Domain III (Figure S2). We tested the additivity of the spectra in the absence and presence of Mg^{2+}. Under both conditions, the CD spectra of $DIII^{core}$ and $DIII^{tail}$ add to give the spectrum of Domain III. This result indicates that the helical composition of the two sub-Domains, $DIII^{core}$ and $DIII^{tail}$, in total, is the same as in intact Domain III.

UV Melting. The UV melting data suggest ground state rRNA structures and unfolding intermediates are composed of independent elements that are not significantly affected by global interactions. Thermal unfolding of RNA, monitored by UV−visible absorbance, can provide estimates of the numbers of transitions and of their thermodynamic parameters. The temperature-induced unfolding transitions of $DIII^{core}$, $DIII^{tail}$, and Domain III were monitored by UV absorbance (Figures 4 and 5). Derivative melting profiles were computed from the data and were fit to unfolding models with independent subtransitions,[24] under two salt conditions for each of the three rRNAs.

$DIII^{core}$, $DIII^{tail}$, and Domain III in Na^{+}. Two wavelengths (260 and 280 nm) were employed to monitor the melting transitions in 180 mM NaCl, 20 mM Tris-HEPES, pH 8.0 buffer solutions. Melting of A-U base pairs is accompanied by a greater

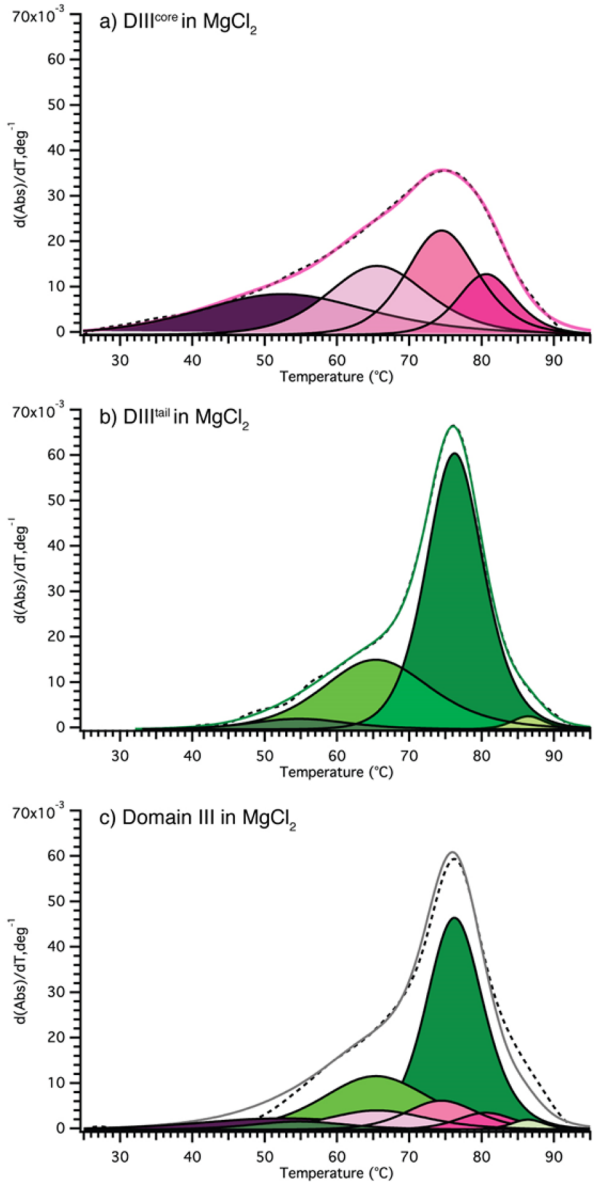

Figure 5. Derivative unfolding profiles along with fit and deconvolution for $DIII^{core}$, $DIII^{tail}$, and Domain III at 260 nm in the presence of Mg^{2+}. Experimental unfolding profiles are indicated by dashed lines. The fits to the unfolding profiles are colored solid lines, and the component transitions are black lines with colored fill. (a) Unfolding profile, fit, and deconvolution of $DIII^{core}$ at 260 nm. (b) Unfolding profile, fit, and deconvolution of $DIII^{tail}$ at 260 nm. (c) Unfolding profile of intact Domain III and the sum of the component transitions of $DIII^{core}$ and $DIII^{tail}$ at 260 nm. The solid line is a weighted sum of the unfolding profiles of $DIII^{core}$ and $DIII^{tail}$. The eight component transitions, obtained from deconvolution of $DIII^{core}$ and $DIII^{tail}$, add to give the unfolding profile of Domain III. All melting experiments were performed in 180 mM NaCl, 0.5 mM $MgCl_2$, 20 mM Tris-HEPES, pH 8.0 buffer.

hyperchromicity at 260 nm, while melting of C-G base pairs has a greater hyperchromicity at 280 nm.[10,24] The fraction of A-U base pairs is relatively low in *T. thermophilus* rRNA and is roughly equivalent in $DIII^{core}$ and $DIII^{tail}$.

The 260 and 280 nm melting profiles were fit independently to unfolding models, for cross-validation of the fits. The same number of transitions, with similar thermodynamic parameters, was obtained at both wavelengths. In general, it can be seen that

DOI: 10.1021/acs.biochem.6b00168
Biochemistry 2016, 55, 4603−4613

Table 1. Estimates of Thermodynamic Parameters for Unfolding of DIII^{core}

transition	T_m (°C)	ΔG (kcal mol^{-1})[a]	ΔH (kcal mol^{-1})	ΔS (cal K^{-1} mol^{-1})	A[b]	A_{260}/A_{280}
1	57.7 ± 3.5[c]	3.9 ± 0.7	39.1 ± 3.6	118 ± 8	3.3 ± 1.8	1.1
	54.9 ± 3.6[d]	3.2 ± 0.8	35.1 ± 3.7	107 ± 9	2.9 ± 1.3	
	53.3 ± 2.4[e]	2.3 ± 0.2	26.7 ± 1.2	81.7 ± 3.1	2.8 ± 0.7	
2	66.9 ± 3.0[c]	8.0 ± 9.9	65.0 ± 37.2	191 ± 78	2.4 ± 3.7	0.9
	66.1 ± 3.0[d]	7.2 ± 7.2	59.5 ± 27.3	175 ± 58	2.7 ± 3.2	
	65.8 ± 2.0[e]	2.8 ± 2.5	49.2 ± 9.6	145 ± 20	2.8 ± 1.6	
3	74.3 ± 0.6[c]	12.5 ± 10.0	88.0 ± 36.0	253 ± 73	3.1 ± 3.1	0.9
	74.2 ± 0.6[d]	11.9 ± 8.9	83.6 ± 32.3	241 ± 66	3.4 ± 3.1	
	74.6 ± 0.8[e]	10.3 ± 4.6	72.2 ± 16.7	208 ± 34	3.0 ± 1.9	
4	80.6 ± 1.0[c]	17.8 ± 6.8	113 ± 24	320 ± 49	1.2 ± 1.0	1.0
	80.6 ± 1.2[d]	16.7 ± 7.1	106 ± 25	300 ± 51	1.2 ± 1.2	
	80.7 ± 0.7[e]	14.7 ± 3.6	93.3 ± 12.8	264 ± 26	1.4 ± 0.9	
totals		42.2 ± 19.4[c]	305 ± 71	882 ± 148		
		39.0 ± 17.0[d]	284 ± 63	823 ± 129		
		30.1 ± 7.7[e]	241 ± 29	699 ± 59		

[a]At 25 °C. [b]Relative hyperchromicity (10×). [c]At 260 nm, with Na^+ only. [d]At 280 nm, with Na^+ only. [e]At 260 nm, with Na^+ and Mg^{2+}.

Table 2. Estimates of Thermodynamic Parameters for Unfolding of DIII^{tail}

transition	T_m (°C)	ΔG (kcal mol^{-1})[a]	ΔH (kcal mol^{-1})	ΔS (cal K^{-1} mol^{-1})	A[b]	A_{260}/A_{280}
1	54.4 ± 4.7[c]	4.3 ± 2.7	48.1 ± 11.7	147 ± 26	0.7 ± 0.7	0.6
	54.1 ± 6.5[d]	3.4 ± 2.1	38.4 ± 9.3	117 ± 21	1.2 ± 1.1	
	55.0 ± 2.8[e]	4.4 ± 1.9	47.6 ± 8.0	145 ± 18	0.4 ± 0.4	
2	64.3 ± 0.5[c]	7.0 ± 2.8	59.8 ± 10.6	177 ± 22	2.8 ± 0.9	1.6
	64.3 ± 0.9[d]	7.0 ± 5.8	59.6 ± 22.1	177 ± 47	1.7 ± 1.3	
	65.7 ± 0.4[e]	5.5 ± 1.2	45.5 ± 4.5	134 ± 10	3.1 ± 0.5	
3	74.6 ± 1.4[c]	15.1 ± 0.7	105 ± 3	303 ± 5	6.1 ± 0.3	0.9
	75.3 ± 0.9[d]	13.7 ± 1.0	94.6 ± 3.5	272 ± 7	6.7 ± 0.4	
	76.3 ± 0.2[e]	13.5 ± 0.2	91.5 ± 0.8	262 ± 2	6.4 ± 0.2	
4	83.3 ± 0.2[c]	25.1 ± 4.5	153 ± 16	429 ± 31	0.5 ± 0.1	0.8
	83.6 ± 0.3[d]	25.6 ± 5.7	156 ± 20	436 ± 40	0.6 ± 0.1	
	86.5 ± 0.1[e]	28.4 ± 4.6	166 ± 16	460 ± 31	0.2 ± 0.0	
totals		51.5 ± 7.5[c]	366 ± 29	1060 ± 60		
		49.7 ± 10.3[d]	349 ± 39	1000 ± 81		
		51.8 ± 5.6[e]	351 ± 21	1000 ± 43		

[a]At 25 °C. [b]Relative hyperchromicity (10×). [c]At 260 nm, with Na^+ only. [d]At 280 nm, with Na^+ only. [e]At 260 nm, with Na^+ and Mg^{2+}.

lower-temperature transitions showed greater hyperchomicities at 260 nm (Figure 4a,c) than at 280 nm (Figure 4b,d). This difference is expected if A-U base pairs melt preferentially at lower temperatures over G-C base pairs. The observed difference is modest because the thermophilic rRNA used here contains a small fraction of A and U nucleotides, and therefore, their contribution to hyperchromicity is low.

DIII^{core}, DIII^{tail}, and Domain III in Na^+ and Mg^{2+}. Mg^{2+} concentrations were restricted (0.50 mM) during the melting of the rRNAs due to degradation in the presence of higher Mg^{2+} concentrations at elevated temperatures. Therefore, the melting transitions were monitored in 180 mM NaCl, 0.5 mM $MgCl_2$, 20 mM Tris-HEPES, pH 8.0 buffer solutions. The addition of 0.5 mM Mg^{2+} to DIII^{core} does not appear to change the number of observable transitions, although the hyperchromicity of a given sample was not fully reproducible because of rRNA degradation. As with DIII^{core}, the addition of 0.5 mM Mg^{2+} to DIII^{tail} does not appear to change the number of observable transitions.

Fitting DIII^{core} and DIII^{tail} Unfolding to Thermodynamic Models. The data fit a model in which DIII^{core} unfolds with four transitions in 180 mM NaCl, 20 mM Tris-HEPES, pH 8.0 buffer in the absence (Figure 4) and presence of 0.5 mM $MgCl_2$ (Figure 5). The thermodynamic parameters obtained from the fits are listed in Table 1. DIII^{tail} also appears to melt with four transitions (Figures 4 and 5 and Table 2). A four-transition model is described by 12 parameters, which are the $T_{m,n}$, ΔH_n, and A_n for each transition n. As noted previously, more complex models with greater numbers of transitions cannot be excluded by the methods used here. The Supporting Information contains a discussion of uncertainties in the models.

The Melting Profile of Domain III Is the Sum of DIII^{core} and DIII^{tail} Melting Profiles. It appears that each of the unfolding transitions of DIII^{core} and DIII^{tail} is conserved in the unfolding of Domain III. The unfolding of Domain III in the presence of Na^+ can be reconstructed by a weighted sum of the component transitions of DIII^{core} and DIII^{tail} (Figure 4e,f). At 260 nm, the weights are given by (0.27)DIII^{core} + (0.71)DIII^{tail} = Domain III. At 280 nm, the weights are given by (0.36)DIII^{core} + (0.69)DIII^{tail} = Domain III. The differences in the weights at 260 and 280 nm appear to be within the error of the experiment. In the presence of Mg^{2+}, it appears that each of the melting transitions of DIII^{core} and DIII^{tail} is generally conserved in the melting of Domain III (Table 3). The melting profile of Domain III in the presence of Mg^{2+} can be roughly reconstructed by a weighted sum of the component transitions of DIII^{core} and DIII^{tail} (Figure 5c). At 260 nm in the presence of Mg^{2+}, the

DOI: 10.1021/acs.biochem.6b00168
Biochemistry 2016, 55, 4603−4613

Table 3. Estimates of Thermodynamic Parameters for Melting of Domain III

transition	T_m (°C)	ΔG (kcal mol^{-1})[a]	ΔH (kcal mol^{-1})	ΔS (cal K^{-1} mol^{-1})	A[b]	A_{260}/A_{280}
1	54.4[c]	4.3	48.1	147	0.5	0.6
	54.1[d]	3.4	38.4	117	0.8	
	53.3[e]	2.3	26.7	81.7	0.8	
2	57.7[c]	3.9	39.1	118	0.9	0.9
	54.9[d]	3.2	35.1	107	1.0	
	55.0[e]	4.4	47.6	145	0.3	
3	64.3[c]	7.0	59.8	177	2.0	1.7
	64.3[d]	7.0	59.6	177	1.2	
	65.7[e]	5.5	45.5	134	2.3	
4	66.9[c]	8.0	65.0	191	0.7	0.7
	66.1[d]	7.2	59.5	175	1.0	
	65.8[e]	2.8	49.2	145	0.8	
5	74.3[c]	12.5	88.0	253	0.8	0.7
	74.2[d]	11.9	83.6	241	1.2	
	74.6[e]	10.3	72.2	208	0.8	
6	74.6[c]	15.1	105	303	4.3	0.9
	75.3[d]	13.7	94.6	272	4.6	
	76.3[e]	13.5	91.5	262	5.0	
7	80.6[c]	17.8	113	320	0.3	0.8
	80.6[d]	16.7	106	300	0.4	
	80.7[e]	14.7	93.3	264	0.4	
8	83.3[c]	25.1	153	429	0.4	1.0
	83.6[d]	25.6	156	436	0.4	
	86.5[e]	28.4	166	460	0.1	
totals		93.7[c]	668	1940		
		88.7[d]	633	1830		
		81.9[e]	592	1700		

[a]At 25 °C. [b]Relative hyperchromicity (10×). [c]At 260 nm, with Na^+ only. [d]At 280 nm, with Na^+ only. [e]At 260 nm, with Na^+ and Mg^{2+}.

weights are given by 0.28(DIII^{core}) + 0.77(DIII^{tail}) = Domain III. The sums of the component transitions, obtained from melting of DIII^{core} and DIII^{tail}, accurately recapitulate the unfolding of Domain III at both wavelengths under both salt conditions. Thus, only two parameters, the weights in the sum, are required to fit the Domain III data to the DIII^{core} and DIII^{tail} unfolding models. Although more complex models cannot be excluded, the simplest model that explains this observation is that in which DIII^{core} and DIII^{tail} are independent within intact Domain III and do not significantly affect each other at any point along the unfolding pathway. The Domain III unfolding pathway does not appear to contain off-pathway unfolding intermediates that are absent from the unfolding pathways of DIII^{core} or DIII^{tail} alone. The combined results support a model in which the unfolding pathway of the rRNA, composed of DIII^{core} and DIII^{tail}, is conserved when Domain III is split into components.

The Summation of the Melting Profiles Is Model-Independent. As described above, the sum of the observed melting profiles of DIII^{core} and DIII^{tail} was fit to the observed profile of Domain III (w_1DIII^{core} + w_2DIII^{tail} = Domain III). Using the weights obtained in that fit (w_1 and w_2), the eight melting transitions, derived from the fits of DIII^{core} and DIII^{tail}, were summed. This weighted summation allowed us to recapitulate the eight-transition unfolding pathway of Domain III. This approach is model-independent in that the summation does not preclude more transitions in the fits of the melting profiles of DIII^{core} and DIII^{tail}. Regardless of the number of transitions used in those fits, the constituent melting transitions of DIII^{core} and DIII^{tail} can be added to recapitulate the melting of Domain III.

DISCUSSION

Large folded RNAs are built from recurrent motifs,[25,26] some of which are of high thermodynamic stability.[27,28] The data here support a model in which not only ground state rRNA structures but also unfolding intermediates are composed of independent elements. Local unfolding is not measurably affected by joining or separating the sub-Domains of Domain III of the LSU rRNA.

RNA unfolding generally follows multistep pathways with observable melting transitions for various junctions, internal helices, and stem–loop motifs. We have fit our thermal melting data to a model in which Domain III unfolds reversibly by eight independent transitions, while isolated DIII^{core} and DIII^{tail} each unfold reversibly via four transitions. For these large RNAs, the number of actual transitions is expected to be greater than estimated by our fitting process.

The data suggest conservation of local unfolding transitions of Domain III and those of the two isolated sub-Domains (Figures 4 and 5). This observation is model-independent and is not dependent on the number of transitions in the fits. Except for small differences that may be attributed to tertiary interactions, the complex multistep melting profiles of DIII^{core} and DIII^{tail} are additive and give the melting profile of Domain III. We do not find evidence that the folding of Domain III involves states that are absent in the folding of isolated DIII^{core} or DIII^{tail}. This result is supported by UV melting data obtained at two wavelengths and under two salt conditions. The thermodynamic parameters for unfolding transitions appear to be conserved whether DIII^{core} or DIII^{tail} is independent or united within Domain III.

Disruption of long-range interactions, when Domain III is cleaved into two sub-Domains, does not appear to significantly impact the folding energetics. The folding intermediates of

DOI: 10.1021/acs.biochem.6b00168
Biochemistry 2016, 55, 4603–4613

the sub-Domains appear to be dominated by local interactions and are less dependent on the surrounding rRNA. Support for conservation of ground state structure, stabilities, and folding mechanisms, upon separation of the sub-Domains, is given by chemical footprinting, equilibrium melting, and CD spectroscopy. Similarity in ground state structures is indicated by comparison of SHAPE reactivities of intact Domain III and isolated sub-Domain $DIII^{core}$. SHAPE reactivities are essentially identical where the sequences correspond. The CD spectra of ground state $DIII^{core}$ and $DIII^{tail}$ add to give the spectrum of Domain III. Additivity of the CD spectra is observed in the absence or presence of Mg^{2+}. Our results indicate dominance of local interactions during folding, not the absence of long-range interactions.

Mg^{2+} Microclusters. The Mg^{2+} dependence of SHAPE reactivities is consistent with the formation of a Mg^{2+} microcluster[15] in both isolated Domain III and $DIII^{core}$. We have previously determined the Mg^{2+} dependence of SHAPE reactivity on a variety of RNAs, including a viral genome,[29] Domain III of the LSU,[16] the central core of the small ribosomal subunit,[3] the P4P6 domain of the *Tetrahymena* ribozyme,[30] and the 23S rRNA (unpublished). The results show that SHAPE is a useful probe of binding of Mg^{2+} to RNA and a suitable assay for formation of tertiary interactions. Mg^{2+} induces changes in SHAPE reactivity at nucleotides that coordinate Mg^{2+} and, in some cases, at nucleotides that are proximal to these Mg^{2+} binding sites.

RNA folding can be constrained by thermodynamics and/or kinetics. Pyle and co-workers report that the unfolding of the long noncoding RNA HOTAIR *in vitro* is irreversible.[31] Folding of this RNA appears to be kinetically controlled. HOTAIR RNA refolds to a nonhomogeneous population that differs from biological HOTAIR. By contrast, rRNA and tRNA folding appears to be thermodynamically controlled. Both modified and native tRNA, along with rRNA, fold reversibly.[24,32] Like tRNA and rRNA, a group I ribozyme, characterized by Woodson,[33] folds reversibly, but unlike tRNA and rRNA, initial steps in the group I ribozyme folding are directed by long-range interactions, between nucleotides that are remote in the secondary structure. tRNA and rRNA folding, by contrast, is driven at early stages by local interactions.

Jaeger,[34] Tan,[35] and others have shown that RNAs can be robust in folding and function. RNA structure can be retained in isolated domains or sub-Domains, and catalytic activity can be regained by assembly in trans. Here we suggest that rRNA and other ancient RNAs may be distinctive, in that independence of rRNA elements is substantially retained in intermediates in complex multistep folding pathways.

Accretion Model. The results obtained here are consistent with our model describing the origin and evolution of rRNA.[1,2] In this model, rRNA grew in size by accretion of small rRNA fragments. The accretion model predicts that rRNA can be decomposed into elements of various granularities, retaining the folding mechanism in isolation.

RNAs in general fold by a variety of mechanistic pathways, which, we suggest, are influenced by their evolutionary histories. A folding pathway may be linear, with a sequential progression, or branched, with an ensemble of intermediates. In either mechanism, intermediates may be nativelike, or not. Native or non-native long-range interactions between secondary elements may be important and can form either early or late in the folding process.

RNA and Protein. Direct comparisons of life's polymers can illuminate and explain some of their most important properties. The experiments here help show how RNA folding differs from protein folding. Proteins fold to autonomous, integrated, and compact structures called domains.[36] A protein domain can be defined as a cooperative thermodynamic unit that is either completely folded or completely unfolded at equilibrium.[37] In general, a native protein domain is destabilized by deletion of component secondary elements,[5,38] consistent with their integration. For example, the removal of a β-sheet from a TIM barrel would abolish folding of the entire barrel.

The architectural logic of RNA differs fundamentally from that of protein. RNA folds locally to small secondary elements, primarily stems and stem−loop motifs. Locally, RNA structure is determined by base pairing, base stacking, rotameric preferences, and interactions with inorganic cations.[39−42] RNA folding, in contrast to protein folding, is hierarchical and is highly influenced by electrostatics; monovalent cations alone favor secondary structure, and addition of divalent cations favors native tertiary structure.[39] In contrast to protein folding, formation of RNA secondary elements is not highly cooperative with global domain assembly; small RNA units are quasi-independent of each other. Therefore, a RNA at equilibrium can occupy partially folded states. RNA can make stepwise transitions between states as the temperature increases. Previously, it has been reported that tRNA,[24,43] mRNA pseudoknots,[8,9] and other RNAs undergo distinct and resolvable transitions during equilibrium melting. These transitions are generally associated with disruption of individual secondary structural elements, which are thermodynamically decoupled after initial (low-temperature) disruption of tertiary interactions.[9,24,43]

RNA−Drug Interactions. The folding competence of isolated rRNA fragments can provide tools for deciphering drug interactions. One example, investigated by the Draper laboratory, is the GTPase-associated region (GAR), a 58-nucleotide rRNA fragment excised from LSU rRNA.[44,45] Isolated GAR folds in the presence of cations to a near-native state and binds to its ribosomal protein partner, rProtein uL11. Formation of the isolated GAR−uL11 complex is blocked by the antibiotic thiostrepton, just as in the assembled ribosome.

■ ASSOCIATED CONTENT

Supporting Information

The Supporting Information is available free of charge on the ACS Publications website at DOI: 10.1021/acs.biochem.6b00168.

Methods on the synthesis and purification of rRNAs, SHAPE data processing, experimental unfolding and their respective residual errors, IGOR fitting equations, and circular dichrosim (PDF)

■ AUTHOR INFORMATION

Corresponding Author

*E-mail: loren.williams@chemistry.gatech.edu. Phone: (404) 385-6258.

Funding

This work was supported by National Aeronautics and Space Administration Grant NNX16AJ29G.

Notes

The authors declare no competing financial interest.

■ ACKNOWLEDGMENTS

The authors thank Jessica Bowman and Poorna Roy for helpful discussions.

DOI: 10.1021/acs.biochem.6b00168
Biochemistry 2016, 55, 4603−4613

■ ABBREVIATIONS

LSU, large ribosomal subunit; rRNA, ribosomal RNA; tRNA, transfer RNA; CD, circular dichroism; SHAPE, selective 2′-hydroxyl acylation analyzed by primer extension; GAR, GTPase-associated region; PDB, Protein Data Bank.

■ REFERENCES

(1) Petrov, A. S., Gulen, B., Norris, A. M., Kovacs, N. A., Bernier, C. R., Lanier, K. A., Fox, G. E., Harvey, S. C., Wartell, R. M., Hud, N. V., and Williams, L. D. (2015) History of the ribosome and the origin of translation. *Proc. Natl. Acad. Sci. U. S. A. 112*, 15396−15401.

(2) Petrov, A. S., Bernier, C. R., Hsiao, C., Norris, A. M., Kovacs, N. A., Waterbury, C. C., Stepanov, V. G., Harvey, S. C., Fox, G. E., Wartell, R. M., Hud, N. V., and Williams, L. D. (2014) Evolution of the ribosome at atomic resolution. *Proc. Natl. Acad. Sci. U. S. A. 111*, 10251−10256.

(3) Gulen, B., Petrov, A. S., Okafor, C. D., Vander Wood, D., O'Neill, E. B., Hud, N. V., and Williams, L. D. (2016) Ribosomal small subunit domains radiate from a central core. *Sci. Rep. 6*, 20885.

(4) Hsiao, C., Lenz, T. K., Peters, J. K., Fang, P. Y., Schneider, D. M., Anderson, E. J., Preeprem, T., Bowman, J. C., O'Neill, E. B., Lie, L., Athavale, S. S., Gossett, J. J., Trippe, C., Murray, J., Petrov, A. S., Wartell, R. M., Harvey, S. C., Hud, N. V., and Williams, L. D. (2013) Molecular paleontology: a biochemical model of the ancestral ribosome. *Nucleic Acids Res. 41*, 3373−3385.

(5) Dyson, H. J., and Wright, P. E. (1993) Peptide Conformation and Protein-Folding. *Curr. Opin. Struct. Biol. 3*, 60−65.

(6) Zen, K. H., McKenna, E., Bibi, E., Hardy, D., and Kaback, H. R. (1994) Expression of lactose permease in contiguous fragments as a probe for membrane-spanning domains. *Biochemistry 33*, 8198−8206.

(7) Johnsson, N., and Varshavsky, A. (1994) Split ubiquitin as a sensor of protein interactions in vivo. *Proc. Natl. Acad. Sci. U. S. A. 91*, 10340−10344.

(8) Gluick, T. C., Wills, N. M., Gesteland, R. F., and Draper, D. E. (1997) Folding of an mRNA pseudoknot required for stop codon readthrough: Effects of mono- and divalent ions on stability. *Biochemistry 36*, 16173−16186.

(9) Stammler, S. N., Cao, S., Chen, S. J., and Giedroc, D. P. (2011) A conserved RNA pseudoknot in a putative molecular switch domain of the 3′-untranslated region of coronaviruses is only marginally stable. *RNA 17*, 1747−1759.

(10) Theimer, C. A., and Giedroc, D. P. (1999) Equilibrium unfolding pathway of an H-type RNA pseudoknot which promotes programmed −1 ribosomal frameshifting. *J. Mol. Biol. 289*, 1283−1299.

(11) Petrov, A. S., Bernier, C. R., Hershkovits, E., Xue, Y., Waterbury, C. C., Hsiao, C., Stepanov, V. G., Gaucher, E. A., Grover, M. A., Harvey, S. C., Hud, N. V., Wartell, R. M., Fox, G. E., and Williams, L. D. (2013) Secondary Structure and Domain Architecture of the 23S rRNA. *Nucleic Acids Res. 41*, 7522−7535.

(12) Sarver, M., Zirbel, C. L., Stombaugh, J., Mokdad, A., and Leontis, N. B. (2007) FR3D: finding local and composite recurrent structural motifs in RNA 3D structures. *J. Math. Biol. 56*, 215−252.

(13) Polikanov, Y. S., Steitz, T. A., and Innis, C. A. (2014) A proton wire to couple aminoacyl-tRNA accommodation and peptide bond formation on the ribosome. *Nat. Struct. Mol. Biol. 21*, 787−793.

(14) Petrov, A. S., Bernier, C. R., Hsiao, C. L., Okafor, C. D., Tannenbaum, E., Stern, J., Gaucher, E., Schneider, D., Hud, N. V., Harvey, S. C., and Williams, L. D. (2012) RNA-Magnesium-Protein Interactions in Large Ribosomal Subunit. *J. Phys. Chem. B 116*, 8113−8120.

(15) Hsiao, C., and Williams, L. D. (2009) A recurrent magnesium-binding motif provides a framework for the ribosomal peptidyl transferase center. *Nucleic Acids Res. 37*, 3134−3142.

(16) Athavale, S. S., Gossett, J. J., Hsiao, C., Bowman, J. C., O'Neill, E., Hershkovitz, E., Preeprem, T., Hud, N. V., Wartell, R. M., Harvey, S. C., and Williams, L. D. (2012) Domain III of the *T. thermophilus* 23S rRNA folds independently to a near-native state. *RNA 18*, 752−758.

(17) Weeks, K. M., and Mauger, D. M. (2011) Exploring RNA Structural Codes with SHAPE Chemistry. *Acc. Chem. Res. 44*, 1280−1291.

(18) Low, J. T., and Weeks, K. M. (2010) SHAPE-directed RNA secondary structure prediction. *Methods (Amsterdam, Neth.) 52*, 150−158.

(19) Wilkinson, K. A., Merino, E. J., and Weeks, K. M. (2006) Selective 2′-hydroxyl acylation analyzed by primer extension (SHAPE): quantitative RNA structure analysis at single nucleotide resolution. *Nat. Protoc. 1*, 1610−1616.

(20) Lipfert, J., Doniach, S., Das, R., and Herschlag, D. (2014) Understanding Nucleic Acid−Ion Interactions. *Annu. Rev. Biochem. 83*, 813−841.

(21) Selmer, M., Dunham, C. M., Murphy, F. V., Weixlbaumer, A., Petry, S., Kelley, A. C., Weir, J. R., and Ramakrishnan, V. (2006) Structure of the 70S ribosome complexed with mRNA and tRNA. *Science 313*, 1935−1942.

(22) Ban, N., Nissen, P., Hansen, J., Moore, P. B., and Steitz, T. A. (2000) The complete atomic structure of the large ribosomal subunit at 2.4 Å resolution. *Science 289*, 905−920.

(23) Hsiao, C., Mohan, S., Hershkovitz, E., Tannenbaum, A., and Williams, L. D. (2006) Single nucleotide RNA choreography. *Nucleic Acids Res. 34*, 1481−1491.

(24) Draper, D. E., Bukhman, Y. V., and Gluick, T. C. (2001) Thermal methods for the analysis of RNA folding pathways. In *Current protocols in nucleic acid chemistry*, 2008/04/23 ed., pp 11.13.11−11.13.13, Wiley, New York.

(25) Moore, P. B. (1999) Structural motifs in RNA. *Annu. Rev. Biochem. 68*, 287−300.

(26) Parlea, L., Sweeney, B. A., Hosseini-Asanjan, M., Zirbel, C. L., and Leontis, N. B. (2016) The RNA 3D Motif Atlas: Computational Methods for Extraction, Organization and Evaluation of RNA Motifs. *Methods (Amsterdam, Neth.) 103*, 99−119.

(27) Antao, V. P., Lai, S. Y., and Tinoco, I., Jr. (1991) A thermodynamic study of unusually stable RNA and DNA hairpins. *Nucleic Acids Res. 19*, 5901−5905.

(28) Mohan, S., Hsiao, C., Bowman, J. C., Wartell, R., and Williams, L. D. (2010) RNA tetraloop folding reveals tension between backbone restraints and molecular interactions. *J. Am. Chem. Soc. 132*, 12679−12689.

(29) Athavale, S. S., Gossett, J. J., Bowman, J. C., Hud, N. V., Williams, L. D., and Harvey, S. C. (2013) In Vitro Secondary Structure of the Genomic RNA of Satellite Tobacco Mosaic Virus. *PLoS One 8*, e54384.

(30) Athavale, S. S., Petrov, A. S., Hsiao, C., Watkins, D., Prickett, C. D., Gossett, J. J., Lie, L., Bowman, J. C., O'Neill, E., Bernier, C. R., Hud, N. V., Wartell, R. M., Harvey, S. C., and Williams, L. D. (2012) RNA Folding and Catalysis Mediated by Iron (II). *PLoS One 7*, e38024.

(31) Somarowthu, S., Legiewicz, M., Chillón, I., Marcia, M., Liu, F., and Pyle, A. M. (2015) HOTAIR Forms an Intricate and Modular Secondary Structure. *Mol. Cell 58*, 353−361.

(32) Sampson, J. R., and Uhlenbeck, O. C. (1988) Biochemical and physical characterization of an unmodified yeast phenylalanine transfer RNA transcribed in vitro. *Proc. Natl. Acad. Sci. U. S. A. 85*, 1033−1037.

(33) Behrouzi, R., Roh, J. H., Kilburn, D., Briber, R. M., and Woodson, S. A. (2012) Cooperative Tertiary Interaction Network Guides RNA Folding. *Cell 149*, 348−357.

(34) Grabow, W. W., Zhuang, Z., Shea, J. E., and Jaeger, L. (2013) The GA-minor submotif as a case study of RNA modularity, prediction, and design. *Wiley Interdisciplinary Reviews: RNA 4*, 181−203.

(35) Pan, T. (1995) Higher order folding and domain analysis of the ribozyme from Bacillus subtilis ribonuclease P. *Biochemistry 34*, 902−909.

(36) Richardson, J. S. (1981) The anatomy and taxonomy of protein structure. *Adv. Protein Chem. 34*, 167−339.

(37) Porter, L. L., and Rose, G. D. (2012) A thermodynamic definition of protein domains. *Proc. Natl. Acad. Sci. U. S. A. 109*, 9420−9425.

(38) Betton, J. M., Desmadril, M., and Yon, J. M. (1989) Detection of intermediates in the unfolding transition of phosphoglycerate kinase using limited proteolysis. *Biochemistry 28*, 5421−5428.

DOI: 10.1021/acs.biochem.6b00168
Biochemistry 2016, 55, 4603−4613

(39) Brion, P., and Westhof, E. (1997) Hierarchy and dynamics of RNA folding. *Annu. Rev. Biophys. Biomol. Struct. 26*, 113−137.
(40) Onoa, B., and Tinoco, I., Jr. (2004) RNA folding and unfolding. *Curr. Opin. Struct. Biol. 14*, 374−379.
(41) Bowman, J. C., Lenz, T. K., Hud, N. V., and Williams, L. D. (2012) Cations in charge: magnesium ions in RNA folding and catalysis. *Curr. Opin. Struct. Biol. 22*, 262−272.
(42) Richardson, J. S., Schneider, B., Murray, L. W., Kapral, G. J., Immormino, R. M., Headd, J. J., Richardson, D. C., Ham, D., Hershkovits, E., Williams, L. D., Keating, K. S., Pyle, A. M., Micallef, D., Westbrook, J., and Berman, H. M. (2008) RNA backbone: Consensus all-angle conformers and modular string nomenclature (an RNA Ontology Consortium contribution). *RNA 14*, 465−481.
(43) Cole, P. E., Yang, S. K., and Crothers, D. M. (1972) Conformational changes of transfer ribonucleic acid. Equilibrium phase diagrams. *Biochemistry 11*, 4358−4368.
(44) Blyn, L. B., Risen, L. M., Griffey, R. H., and Draper, D. E. (2000) The RNA-binding domain of ribosomal protein L11 recognizes an rRNA tertiary structure stabilized by both thiostrepton and magnesium ion. *Nucleic Acids Res. 28*, 1778−1784.
(45) Conn, G. L., Draper, D. E., Lattman, E. E., and Gittis, A. G. (1999) Crystal structure of a conserved ribosomal protein-RNA complex. *Science 284*, 1171−1174.

DOI: 10.1021/acs.biochem.6b00168
Biochemistry 2016, 55, 4603−4613